Broad-Band Microwave Characterization of Bilayered Materials Using a Coaxial Discontinuity with Applications for Thin Conductive Films for Microelectronics and Material in Air-Tight Cell

Nour-eddine Belhadj-Tahar, Olivier Meyer, and Arlette Fourrier-Lamer

***Abstract*—A new measurement method of complex permittivity of bilayered materials has been developed using a coaxial discontinuity. The electromagnetic analysis is performed according to the "mode-matching" method. The reflection coefficient of the principal transverse electromagnetic (TEM) mode is calculated by matching the fields at the interfaces of the layered material and using the orthogonality properties of modes in cylindrical waveguides. The complex permittivity of several known liquid or solid materials in bilayered structure are measured using this method. The experimental results over a wide frequency band (1 kHz–18 GHz) are consistent with those in previous papers and with dc measurements.**

***Index Terms*—Bilayered materials, broad-band measurements, coaxial discontinuity, microwave characterization, mode-matching method.**

I. Introduction

THERE is an increasing interest in broad-band measurement of the complex permittivity of materials in layered structures. The knowledge of thin films permittivity is essential in microelectronics since their performances are related to their frequency behavior. Other applications are also encountered in tight media where the measurement of permittivity shows the evolution of the state of matter with temperature and time and enables the following of the physical process.

Due to its relative simplicity, the transmission/reflection (TR) method is presently the widely used broad-band measurement technique [1]. This method, where a sample of the material to be tested is inserted in a waveguide or a transmission line such as a coaxial or planar line, is nevertheless limited in frequency. The increase in frequency is limited by the appearance of resonance phenomena due to the sample length. The explicit solution for permittivity determined from measured reflection coefficient leads to an ill-conditioned set of equations when the sample length is equal to an integral number of half-wavelengths inside the sample. To bypass this problem, a short sample can be used. However, the use of short samples lowers the measurement sensitivity [2] which makes this method inadequate for the thin film's measurement. Iterative algorithms are also used (i.e., [2] and [3]) to find more precise permittivity estimations. Another problem encountered in practice is the air gap near the inner conductor for the method where a test specimen is inserted in a precision coaxial air line. It is shown in [4] that air-gap errors become more and more serious with increasing dielectric constants. A coaxial capacitor model for air-gap corrections is used in [5].

Open-ended coaxial lines are commonly used as electromagnetic probes for nondestructive testing. The method has been found to satisfactorily work for liquid measurements where good contact between sample and probe is easily obtained [6]. A noncontacting probe has recently been proposed [7] for particular nondestructive industrial applications and can be used for the layered problem.

The purpose of this paper is to outline a broad-band measurement technique for bilayered materials in confined media. The method proposed here uses the inner-coaxial conductor discontinuity into which the cylindrical sample to be measured is easily inserted. The problem analysis is based on the presence of higher-order modes in materials to be tested and excited by the coaxial discontinuity [8]. The capacitive nature of these higher-order modes of transverse magnetic (TM) type and their evanescent character allow permittivity measurements from low frequencies up to 18 GHz in APC-7 mm standard and 40 GHz in APC-2.4 mm standard on samples with thickness greater than 0.1 μm. The method is best suited for various scientific applications, where only small quantities of materials are available.

II. Direct Problem

A. Formulation of the Problem

The proposed structure is depicted in Fig. 1. The coaxial air line (A region) is loaded by a circular waveguide. This circular waveguide is filled with a bilayered material and a short-circuited back side. Both layers 1 and 2 (B and C regions) are assumed isotropic and nonmagnetic. The relative primitivities ε_1 and ε_2 are dimensionless numbers in general are complex and frequency-dependent.

Let us consider an incident transverse electromagnetic (TEM) wave in the coaxial line. At the $z = 0$ plane, the structure may be represented by a coaxial line terminated by an admittance y_e normalized in relation to the characteristic admittance of the coaxial line (Fig. 2). The direct problem

Manuscript received February 16, 1996; revised October 18, 1996.

The authors are with the Laboratoire de Dispositifs Infrarouge et Micro-ondes (LDIM-EA253/DSPT4/MESR), Université Pierre et Marie Curie, 75252 Paris Cedex 05, France.

Publisher Item Identifier S 0018-9480(97)00831-4.

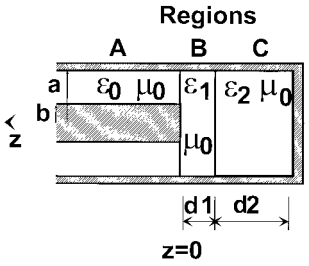

Fig. 1. Cross section of the studied structure.

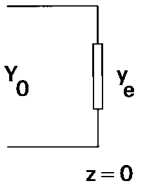

Fig. 2. Equivalent representation of the structure.

involves the y_e determination by a modal analysis combined with the mode-matching method.

B. Fields in the Structure

The nature of the TEM mode and the cylindrical symmetry of Fig. 1 enable us to predict that only higher-order modes of type TM independent of the azimuthal angle F are excited at the geometrical discontinuity plane $z = 0$.

In the coaxial line (A region), the components of the total electromagnetic field are

$$E_{rA} = \frac{1}{r}A_0[\exp(jk_0z) + \Gamma\exp(-jk_0z] + \sum_{m=1}^{\infty} A_m Z_1(\pi_m r)\exp(-\gamma_{Am}z) \quad (1)$$

$$E_{zA} = \sum_{m=1}^{\infty} A_m \frac{\pi_m}{\gamma_{Am}} Z_0(\pi_m r)\exp(-\gamma_{Am}z) \quad (2)$$

$$H_{\Phi A} = \frac{1}{r}A_0 Y_{A0}[\exp(jk_0z) - \Gamma\exp(-jk_0z] + \sum_{m=1}^{\infty} A_m Y_{Am} Z_1(\pi_{Am}r)\exp(-\gamma_{Am}z) \quad (3)$$

where a time dependence of $\exp(j\omega t)$ is assumed, with $\omega = 2\pi f$ and f the operating frequency. A_0 represents the incident TEM wave amplitude and Γ its reflection coefficient at the $z = 0$ plane. Y_{A0} and Y_{Am} are, respectively, the wave admittances of the TEM and TM_{0m} in the coaxial waveguide

$$Y_{A0} = -\sqrt{\frac{\varepsilon_0}{\mu_0}} \quad (4)$$

$$Y_{Am} = \frac{j\omega\varepsilon_0}{\gamma_{Am}} \quad (5)$$

with ε_0 and μ_0 the permittivity and permeability of free space

$$k_0 = \omega\sqrt{\varepsilon_0\mu_0} \quad (6)$$

and

$$\gamma_{Am} = \sqrt{\pi_m^2 - k_0^2}. \quad (7)$$

In (1)–(3), Z_i represents the linear combination of the ith order Bessel functions of the first and second kinds as follows:

$$Z_i(\pi_m r) = J_i(\pi_m r) + G_{Am}N_i(\pi_m r). \quad (8)$$

In the first layer (B region)

$$E_{rB} = \sum_{n=1}^{\infty} B_n J_1(\lambda_n r)[\exp(\gamma_{Bn}z) + \Gamma_n\exp(-\gamma_{Bn}z)] \quad (9)$$

$$E_{zB} = \sum_{n=1}^{\infty} B_n \frac{\lambda_n}{\gamma_{Bn}} J_0(\lambda_n r)[\exp(\gamma_{Bn}z) - \Gamma_n\exp(-\gamma_{Bn}z)] \quad (10)$$

$$H_{\Phi B} = \sum_{n=1}^{\infty} Y_{Bn}B_n J_1(\lambda_n r)[\exp(\gamma_{Bn}z) - \Gamma_n\exp(-\gamma_{Bn}z)] \quad (11)$$

where Γ_n represents the reflection coefficient of the TM_{0n} higher-order mode in the first layer at the $z = 0$ plane, and Y_{Bn} the admittance of this mode

$$Y_{Bn} = -j\frac{\omega\varepsilon_0\varepsilon_1}{\gamma_{Bn}} \quad (12)$$

with

$$\gamma_{Bn} = \sqrt{\lambda_n^2 - k_0^2\varepsilon_1}. \quad (13)$$

In the second layer (C region)

$$E_{rC} = \sum_{p=1}^{\infty} C_p J_1(\chi_p r)sh[\gamma_{Cp}(z + d_1 + d_2)] \quad (14)$$

$$E_{zC} = \sum_{p=1}^{\infty} C_p \frac{\chi p}{\gamma_{Cp}} J_0(\chi_p r)ch[\gamma_{Cp}(z + d_1 + d_2)] \quad (15)$$

$$H_{\Phi C} = \sum_{p=1}^{\infty} Y_{Cp}C_p J_1(\chi_p r)ch[\gamma_{Cp}(z + d_1 + d_2)] \quad (16)$$

with

$$Y_{Cp} = -j\frac{\omega\varepsilon_0\varepsilon_2}{\gamma_{Cp}} \quad (17)$$

and

$$\gamma_{Cp} = \sqrt{\chi_p^2 - k_0^2\varepsilon_2}. \quad (18)$$

The E_z axial component of the electrical field for each TM mode must be zero at the conductors in the three regions. The following conditions are thus obtained by canceling the relations (2), (10), and (15):

$$Z_0(\pi_m a) = Z_0(\pi_m b) = 0 \quad (19)$$

$$J_0(\lambda_n a) = 0 \quad (20)$$

$$J_0(\chi_p a) = 0. \quad (21)$$

Equation (19) enables us to determine the coefficient G_{Am} contained in (8)

$$G_{Am} = -\frac{J_0(\pi_m a)}{N_0(\pi_m a)} = -\frac{J_0(\pi_m b)}{N_0(\pi_m b)} \quad (22)$$

and, thus, from the following transcendental equation, we obtain the coefficients π_m:

$$J_0(\pi_m a)N_0(\pi_m b) - J_0(\pi_m b)N_0(\pi_m a) = 0. \quad (23)$$

The constants λ_n and χ_p are obtained by solving (20)–(21). Note that λ_n and χ_p are equal for $n = p$.

From the relations (9), (11), (1), and (3) the boundary conditions for the transverse components at the $z = 0$ plane are written in the following manner:

$$E_{rB} = 0 \qquad 0 < r < b \quad (24)$$

$$E_{rB} = \sum_{n=1}^{\infty} B_n J_1(\lambda_n r)[1+\Gamma_n] = \frac{1}{r}A_0[1+\Gamma] + \sum_{m=1}^{\infty} A_m Z_1(\pi_m r) \qquad b < r < a \quad (25)$$

$$H_{\Phi B} = \sum_{n=1}^{\infty} Y_{Bn} B_n J_1(\lambda_n r)[1-\Gamma_n] \qquad b < r < a$$

$$= \frac{1}{r}A_0 Y_{A0}[1-\Gamma] + \sum_{m=1}^{\infty} A_m Y_{Am} Z_1(\pi_m r). \quad (26)$$

The coefficients A_m and B_n are determined by using the orthogonality properties of Bessel functions.

The first step consists of performing the integrals $\int_0^a rJ_1(\lambda_n r)E_{rB}\,dr$. The substitution of E_{rB} from (24) and (25) in the above integral yields

$$\frac{B_n[1+\Gamma_n]}{\lambda_n} = A_0[1+\Gamma]\frac{2J_0(\lambda_n b)}{\lambda_n^2 a^2 J_1^2(\lambda_n a)} \cdot \left[1 - \sum_{m=1}^{\infty} \frac{A_m}{A_0(1+\Gamma)} \frac{bZ_1(\pi_m b)}{\frac{\pi_m^2}{\lambda_n^2} - 1}\right] \quad (27)$$

for $n = 1, 2, 3 \cdots$.

Next, we integrate $H_{\Phi B}$ between $r = b$ and $r = a$. We obtain from (26)

$$Y_{A0}A_0[1-\Gamma]\ln\left(\frac{a}{b}\right) = \sum_{n=1}^{\infty} \frac{Y_{Bn}B_n}{\lambda_n}[1-\Gamma_n]J_0(\lambda_n b). \quad (28)$$

At the $z = 0$ plane the input admittance normalized in relation to the characteristic admittance of the coaxial waveguide is

$$y_e = \frac{1-\Gamma}{1+\Gamma} \quad (29)$$

so (27) and (28) give us the result

$$y_e = j\frac{2k_0 a\varepsilon_1}{\ln\left(\frac{a}{b}\right)} \sum_{n=1}^{\infty} \frac{J_0^2(\lambda_n b)}{[\lambda_n^2 a^2 J_1^2(\lambda_n a)]\sqrt{\lambda_n^2 a^2 - k_0^2 a^2 \varepsilon_1}} \cdot \frac{1-\Gamma_n}{1+\Gamma_n}\left[1 - \sum_{m=1}^{\infty} \frac{A_m}{A_0(1+\Gamma)} \frac{bZ_1(\pi_m b)}{\frac{\pi_m^2}{\lambda_n^2} - 1}\right]. \quad (30)$$

This may be written in the form

$$y_e = j\frac{2k_0 a\varepsilon_1}{\ln\left(\frac{a}{b}\right)}\left(y_0 - \sum_{m=1}^{\infty} x_m y_m\right) \quad (31)$$

where y_0, x_m, and y_m are defined as

$$y_0 = \sum_{n=1}^{\infty} \frac{1-\Gamma_n}{1+\Gamma_n} \frac{1}{\lambda_n^2 a^2 \sqrt{\lambda_n^2 a^2 - k_0^2 a^2 \varepsilon_1}} \frac{J_0^2(\lambda_n b)}{J_1^2(\lambda_n a)} \quad (32)$$

$$x_m = \frac{A_m}{A - 0(1+\Gamma)} bZ_1(\pi_m b) \quad (33)$$

$$y_m = -\sum_{n=1}^{\infty} \frac{1-\Gamma_n}{1+\Gamma_n} \frac{1}{(\lambda_n^2 a^2 - \pi_m^2 a^2)\sqrt{\lambda_n^2 a^2 - k_0^2 a^2 \varepsilon_1}} \cdot \frac{J_0^2(\lambda_n b)}{J_1^2(\lambda_n a).} \quad (34)$$

In (31)–(34), Γ_n and x_m are still unknown.

Γ_n is computed by using orthogonality properties of TM modes in the cylindrical waveguide. The total electromagnetic field in the B and C regions is matched at the plane $z = -d_1$. Referring to (9), (11), (14), and (16) we have

$$E_{rB} = \sum_{n=1}^{\infty} B_n J_1(\lambda_n r)[\exp(-\gamma_{Bn}d_1) + \Gamma_n \exp(\gamma_{Bn}d_1)] = \sum_{p=1}^{\infty} C_p J_1(\chi_p r) sh(\gamma_{Cp}d_2) \quad (35)$$

$$H_{\Phi B} = \sum_{n=1}^{\infty} Y_{Bn} B_n J_1(\lambda_n r)[\exp(-\gamma_{Bn}d_1) - \Gamma_n \exp(\gamma_{Bn}d_1)] = \sum_{p=1}^{\infty} Y_{Cp} C_p J_1(\chi_p r) ch(\gamma_{Cp}d_2). \quad (36)$$

The above relations are used to perform the integrals $\int_0^a rJ_1(\lambda_n r)E_{rB}\,dr$ and $\int_0^a rJ_1(\lambda_n r)H_{\Phi B}\,dr$. Integrating and using (12) and (17), we may write

$$B_n[\exp(-\gamma_{Bn}d_1) + \Gamma_n \exp(\gamma_{Bn}d_1)] = C_p sh(\gamma_{Cp}d_2) \quad \text{for} \quad n = p \quad (37)$$

$$\frac{\varepsilon_1}{\gamma_{Bn}} B_n[\exp(-\gamma_{Bn}d_1) - \Gamma_n \exp(\gamma_{Bn}d_1) = \frac{\varepsilon_2}{\gamma_{Cp}} C_p ch(\gamma_{Cp}d_2) \quad \text{for} \quad n = p \quad (38)$$

with

$$\gamma_{Bn} = \sqrt{\lambda_n^2 - k_0^2 \varepsilon_1} \quad (39)$$

$$\gamma_{Cp} = \sqrt{\chi_p^2 - k_0^2 \varepsilon_2} \quad (40)$$

and

$$\chi_p = \lambda_n \quad \text{for} \quad n = p. \quad (41)$$

Combining (37) and (38) the value of Γ_n is then found (see (42) at shown at the bottom of the next page).

The unknowns x_m are found from (26) if the integration of the quantity $rZ_1(\pi_m r)H_{\Phi B}$ is made between $r = b$ and $r = a$. The result is

$$\frac{Y_{Aq}}{2}A_q bZ_1(\pi_q b)\left[\frac{a^2Z_1^2(\pi_q a)}{b^2Z_1^2(\pi_q b)}-1\right] = \sum_{n=1}^{\infty}\frac{Y_{Bn}B_n\lambda_n J_0(\lambda_n b)}{\lambda_n^2-\pi_q^2}[1-\Gamma_n]. \quad (43)$$

If Y_{Aq}, Y_{Bn}, and B_n are substituted with (5), (12), and (27) in (43), it may be shown that

$$\frac{1}{4\varepsilon_1\sqrt{\pi_q^2a^2-k_0^2a^2}}\frac{A_q}{A_0[1+\Gamma]}bZ_1(\pi_q b)\left[\frac{a^2Z_1^2(\pi_q a)}{b^2Z_1^2(\pi+qb)}-1\right] = -\sum_{n=1}^{\infty}\frac{\lambda_n^2a^2}{(\lambda_n^2a^2-\pi_q^2a^2)\sqrt{\lambda_n^2a^2-k_0^2\varepsilon_1}a^2}\frac{1-\Gamma_n}{1+\Gamma_n} \cdot\frac{J_0^2(\lambda_n b)}{J_1^2(\lambda_n a)}\left[1-\sum_{m=1}^{\infty}\frac{A_m}{A_0(1+\Gamma)}\frac{bZ_1(\pi_m b)}{\pi_m^2a^2-\lambda_n^2a^2}\right] \quad (44)$$

or most conveniently

$$\sum_{m=1}^{\infty}A_{mq}x_m = y_q \qquad q=1,2,\cdots \quad (45)$$

by setting (see (46) at bottom of the page) where δ_{mq} is the Kronecker delta function and y_q is found by (34).

C. Numerical Computation

The y_e computation (32) starts with the evaluation of quantities π_m, λ_n, and χ_p from a Bessel subroutine. The roots of the transcendental equations (23), (20), and (21) are found by iteration. It can be shown that all these roots (π_m, λ_n, and χ_p) are real even in the lossy case (lossy materials in regions B and C), and so the arguments of the calculated Bessel functions are real. These functions are programmed in the polynomial approximation form [9] with an absolute accuracy of 10^{-8}. Hence, for a given frequency and for two layers of known electrical properties Γ_n (42), y_0 (32), and y_m (34) can be conveniently processed if the infinite series involved are truncated. This truncation recurs to retaining a finite number of higher-order modes excited by the inner-coaxial conductor discontinuity at $z = 0$. Hence, we retain a N number of TM_{0n} modes in the two-layer structure

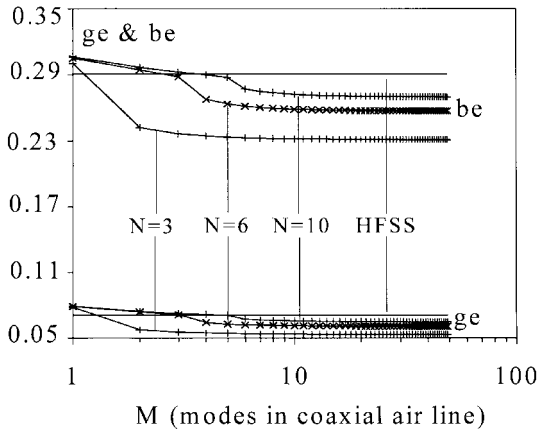

Fig. 3. Variations of the admittance $y_e = g_e + jb_e$ vs M for various values of N at 1 GHz. The simulation uses $a = 3.5$ mm and $b = 1.52$ mm, with $d_1 = 0.5\mathrm{mm}, d_2 = 14\mathrm{mm}, \epsilon_1 = 9.6$ (alumina window), and $\epsilon_2 = 14.78 - j10.43$.

$(n = 1,2,\cdots,N)$. In the same manner, to compute the unknowns x_m, we consider a M number of TM_{0m} modes in the coaxial line $(m = 1,2,\cdots,M)$. Hence (45) is reduced to a system of M equations with M unknowns x_m. From this, y_e is obtained. Since the value of M governs the number of simultaneous equations to be solved, it is clear that for a solution of given accuracy there will be a considerable saving of computer time and storage if the ratio N/M is correctly chosen. The effect on the admittance computation accuracy of the number of higher-order modes retained has been described in [10] and reported by other authors [11]–[12]. Fig. 3 shows the variations with M of the admittance y_e for various values of N. In order to check the correctness of admittance value computed for this case, a comparison was made with value calculated by the finite element method (HP 85 180A High-Frequency Structure Simulator [HFSS]). There is uniform convergence of the normalized values of conductance g_e and susceptance b_e for M increasing. Changes of slope being shown near the HFSS's value for $M > N/2$. The reason of the change of slope can be explained as follows. The magnetic field distribution in the cylindrical waveguide is known as the function of the TEM mode (28). The electric field for a given TM_{0n} mode in the cylindrical waveguide is determined by a series of electric fields of coaxial TM_{0m} modes (27). The amplitude of the magnetic field of each coaxial TM_{0m} mode is

$$\Gamma_n = \frac{\frac{\varepsilon_1}{\sqrt{\lambda_n^2-k_0^2\varepsilon_1}}-\frac{\varepsilon_2}{\sqrt{\lambda_n^2-k_0^2\varepsilon_2}}\coth(d_2\sqrt{\lambda_n^2-k_0^2\varepsilon_2})}{\frac{\varepsilon_1}{\sqrt{\lambda_n^2-k_0^2\varepsilon_1}}+\frac{\varepsilon_2}{\sqrt{\lambda_n^2-k_0^2\varepsilon_2}}\coth(d_2\sqrt{\lambda_n^2-k_0^2\varepsilon_2})}\exp(-2d_1\sqrt{\lambda_n^2-k_0^2\varepsilon_1}) \quad (42)$$

$$A_{mq} = \sum_{n=1}^{\infty}\frac{\lambda_n^2a^2}{(\lambda_n^2a^2-\pi_q^2a^2)(\lambda_n^2a^2-\pi_m^2a^2)\sqrt{\lambda_n^2a^2-k_0^2\varepsilon^2a^2}}\frac{1-\Gamma_nJ_0^2(\lambda_n b)}{1+\Gamma_nJ_1^2(\lambda_n a)}+\frac{1}{\varepsilon_1}\frac{\delta_{mq}}{4\sqrt{\pi_q^2a^2-k_0^2a^2}}\left[\frac{a^2Z_1^2(\pi_q a)}{b^2Z_1^2(\pi_q b)}-1\right] \quad (46)$$

derived from (43) by a series of magnetic fields of cylindrical waveguide modes. The predominant term in the mode series in (43) will be that for which the values of π_m and λ_n are close. If these quantities are expressed as [13]

$$\pi_m(a-b) \approx m\pi \tag{47}$$

$$\lambda_n a \approx \frac{\pi}{4}(4n-1) \tag{48}$$

then

$$\frac{4m}{4n-1} \approx 1 - \frac{b}{a}. \tag{49}$$

In this case, both TM_{0m} and TM_{0n} have the same cutoff wavelength and also the same field variation across the $z = 0$ discontinuity (for a 50 Ω coaxial air-line, $1 - b/a = 0.56$, and $m \approx 0.56n$). If N modes are retained in the circular waveguide, magnetic field distribution in this region is known exactly [see (28)], being that the TEM mode is independent of the calculation process. In (43), the excess modes TM_{oq} with $q > (1 - b/a)N$ have small amplitude coefficients and are effectively ignored. The accuracy of the solution is not affected by an excess of coaxial modes and so the ratio M/N of integers should be chosen slightly less than $1 - b/a$ ($M/N = 0.5$ for the 50 Ω coaxial air-line). Fig. 4 shows that the convergence rate is improved when the ratio N/M corresponds to the ratio of spatial frequencies of the highest-order modes on either side of the junction and convergence is sufficient after only three modes in the small waveguide. For a discontinuity in a 50 Ω coaxial air line, all computations are performed with $N = 6$ and $M = 3$. In Fig. 5 is shown measured and calculated admittance $y_e = g_e + jb_e$ of a bilayered structure formed by an alumina window ($d_1 = 0.5$ mm) and distilled water ($d_2 = 14$ mm). Measurements are performed from 45 MHz–18 GHz at 20°C using an APC-7 mm coaxial air line. The dielectric properties of distilled water are summarized from [14] by the equation (Cole–Cole representation)

$$\varepsilon_2(\omega) = \varepsilon_\infty + \frac{\varepsilon_S - \varepsilon_\infty}{1 + \left(j\dfrac{\omega}{\omega_0}\right)^{1-\alpha}} \tag{50}$$

with parameters values summarized in Table I. Alumina shows very small losses (ε'' is lower less than 0.001) and an ε' value of 9.6 according to [15].

III. Inverse Problem and Experimental Results

In this section, we consider two practical cases.

1) Dielectric properties are known for layer 1 and unknown for layer 2. This configuration constitutes a tight cell and is used for complex permittivity measurements of liquids and semisolids as shown in Fig. 1.
2) Dielectric properties are unknown for layer 1 and known for layer 2. This structure is used for measurements of the permittivity of thin films coated on dielectric substrates.

The measurements presented are obtained at 20°C using the HP8510B network analyzer in a APC-7 mm standard air line. To avoid contact effects the samples are metallized on contact surfaces with line conductors.

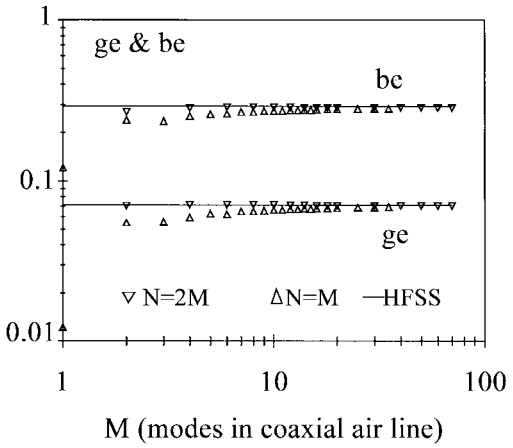

Fig. 4. Variations of the admittance $y_e = g_e + jb_e$ vs M for two ratios N/M at 1 GHz. The simulation uses $a = 3.5$ mm and $b = 1.52$ mm, with $d_1 = 0.5$ mm, $d_2 = 14$ mm, $\epsilon_1 = 9.6$ (alumina window), and $\epsilon_2 = 14.78 - j10.43$.

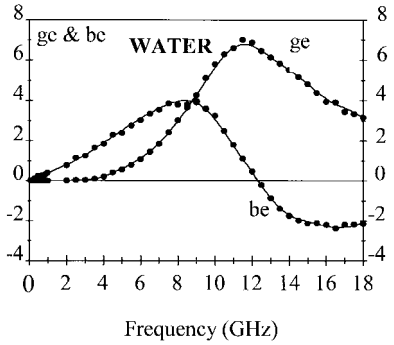

Fig. 5. Measured (o) and calculated $(-)$ admittance $y_e = g_e + jb_e$ of a bilayered structure formed by an alumina window ($d_1 = 0.5$ mm) and distilled water ($d_2 = 14$ mm) in APC-7 mm standard.

TABLE I
Dispersion Parameters Used with (50) To Calculate The Permittivity of Liquids Measured in this Study

Liquids	ε_∞	ε_s	$\omega_0 / 2\pi$ (GHz)	α
water	5.2	80.4	17.0	0
methanol	5.7	33.64	3.0	0
ethanol	4.2	25.07	1.1	0

Temperature is 20°C.

Values from [14].

If $\varepsilon_i = \varepsilon_i' - j\varepsilon_i''$ ($i = 1$ or 2) is the complex permittivity of the unknown layer, the simultaneous determination of ε_i' and ε_i'' is carried out from measured $y_e = g_e + jb_e$ values. For this purpose we use an iterative method derived from the gradient method [16]. Let us consider an initial vector

$$\vec{U}_0 = \begin{bmatrix} \varepsilon_i' \\ \varepsilon_i'' \end{bmatrix} \tag{51}$$

where we define an error vector $\Delta\vec{y}_e$ in the following manner:

$$\Delta\vec{y}_e = \begin{bmatrix} g_e^{(m)} - g_e^{(c)} \\ b_e^{(m)} - b_e^{(c)} \end{bmatrix} \tag{52}$$

where the superscripts m and c denote, respectively, the measured and calculated admittance values. At the $\Delta\vec{y}_e$ vector, we associate a second vector $\Delta\vec{U}$ as follows:

$$\Delta\vec{y}_e = [D]\Delta\vec{U} \tag{53}$$

where the matrix $[D]$ is defined as the derivative matrix

$$[D] = \begin{bmatrix} \dfrac{\partial g_e^{(c)}}{\partial \varepsilon' i} & \dfrac{\partial g_e^{(c)}}{\partial \varepsilon'' i} \\ \dfrac{\partial b_e^{(c)}}{\partial \varepsilon' i} & \dfrac{\partial b_e^{(c)}}{\partial \varepsilon'' i} \end{bmatrix} \tag{54}$$

and

$$\Delta\vec{U} = \begin{bmatrix} \Delta\varepsilon' i \\ \Delta\varepsilon'' i \end{bmatrix}. \tag{55}$$

The $\Delta\vec{U}$ vector value is obtained from the inverse matrix $[D]^{-1}$ as follows:

$$\Delta\vec{U} = [D]^{-1}\Delta\vec{y}_e. \tag{56}$$

The nth direction of investigation is now

$$\vec{U}_n = \vec{U}_{n-1} + \alpha_n \begin{bmatrix} \Delta\varepsilon' i \\ \Delta\varepsilon'' i \end{bmatrix}. \tag{57}$$

α_0 is initialized at 0.2. The coefficient α_n is equal to $2\alpha_{n-1}$ (0.9 at maximum) if $||\Delta\vec{y}_e||_n$ $||\Delta\vec{y}_e||_{n-1}$, else $\alpha_n = \alpha_{n-1}/10$. Iterations are stopped when $||\Delta\vec{y}_e||_n$ is lower than 10^{-9} or α_n lower than 10^{-3}. These values are fixed by the accuracy of the network analyzer. The calculated ε_i' and ε_i'' values become the initial values for the next measured point. The typical computation time for 201 frequency measured points is less than 30 s using a HP 715-75 workstation.

To illustrate this method, we begin with measurements conducted on two reference liquids: ethanol and methanol. In this case, layer 1 is alumina and constitutes a tight dielectric window which separates the liquid (layer 2) from the coaxial line. Alumina and the reference liquid have a thickness of 0.5 mm and 14 mm, respectively. The first step is to measure the window permittivity. This determination is performed by measuring the admittance y_e of the empty tight cell. The inverse problem is solved by assuming that the permittivity ε_1 of alumina is unknown and that the permittivity ε_2 of air is equal to unity. The result (shown in Fig. 6) is in good agreement with [15]. The cell is now filled with the liquid and its admittance is measured with the same procedure used for the empty cell. The window characteristics being known, resolution of the inverse problem gives us the reference liquid permittivity. Figs. 7 and 8 illustrate the results for methanol and ethanol. Our results are found to be in excellent agreement with [17] and the dielectric properties predicted by [14] and reported in Table I.

Next, we shall consider the results for the officinal Vaseline given in Fig. 9. The configuration adopted here is: the officinal Vaseline constitute layer 1 with $d_1 = 0.5$ mm and layer 2 is the alumina studied above (Fig. 6) with $d_2 = 0.5$ mm. These results show a very good agreement with values $\varepsilon_2' = 2.16$ and $\varepsilon_2'' < 2\ 10^{-3}$ according to [18].

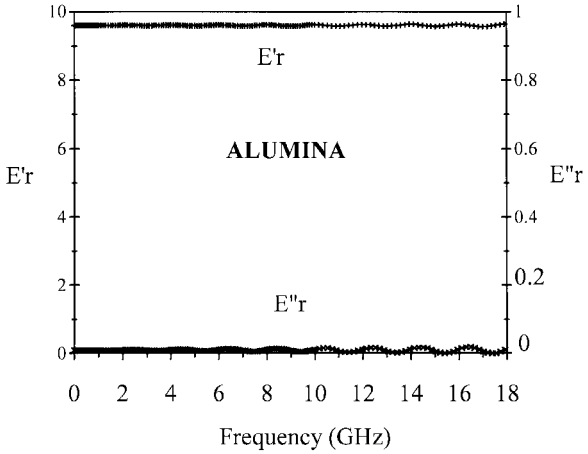

Fig. 6. Complex permittivity of alumina measured in the tight bilayered structure formed by the alumina window ($d_1 = 0.5$ mm) and air ($d_2 = 14$ mm) in APC-7 mm standard.

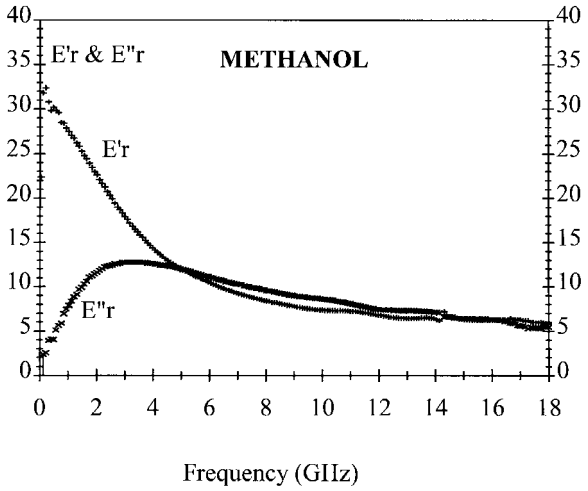

Fig. 7. Complex permittivity of methanol measured in the tight bilayered structure formed by the alumina window ($d_1 = 0.5$ mm) and methanol ($d_2 = 14$ mm) in APC-7 mm standard.

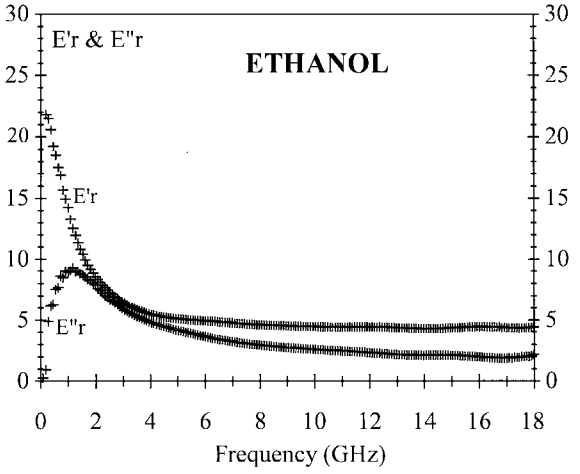

Fig. 8. Complex permittivity of ethanol measured in the tight bilayered structure formed by the alumina window ($d_1 = 0.5$ mm) and ethanol ($d_2 = 14$ mm) in APC-7 mm standard.

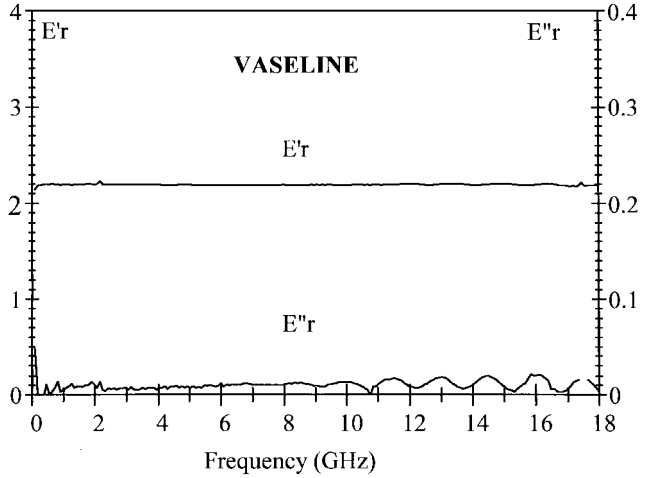

Fig. 9. Complex permittivity of the officinal Vaseline measured in the bilayered structure formed by Vaseline ($d_1 = 0.5$ mm) and alumina ($d_2 = 0.5$ mm) in APC-7 mm standard.

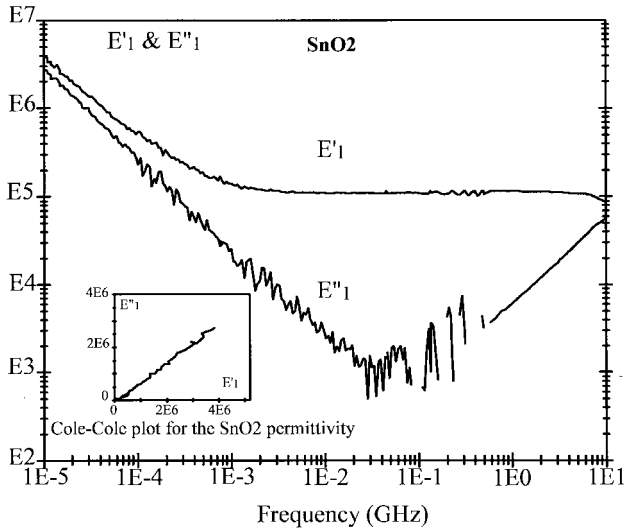

Fig. 10. Complex permittivity of SnO_2 measured in the bilayered structure formed by the film of SnO_2 ($d_1 = 0.25$ μm) coating an substrate of glass ($d_2 = 1$ mm and $\varepsilon_2 = 7.1 - j0.2$) in APC-7mm standard.

A final validation has been made for high conductive film (layer 1) coating a dielectric substrate (layer 2). Thickness of polycrystalline stannic oxide film, SnO_2, is 0.25 μm. The substrate is a glass which shows a permittivity $\varepsilon_2 = 7.1 - j0.2$ (these average values are measured by the method described in [19]). The results for ε_1 and σ_1 are depicted in Figs. 10 and 11 (ac conductivity is defined as $\omega\varepsilon_0\varepsilon_1''$). The measured dc conductivity performed on the crystalline sample is 10^5 S/m and presents a high discrepancy between both measurements. The strong dispersion at low frequencies (corresponding to data between 10 kHz–1 MHz) is related to interfacial polarizations between the stannic oxide film and the electrodes [20] as shown in the Cole–Cole representation in Fig. 10. At high frequencies ε_1'' increases with increasing frequency, while the abnormally high value of ε_1' first is constant and then decreases from 8 GHz. This is the typical variation with frequency of apparent permittivity for polycrystalline materials due to the presence of grain boundaries within the material (see for example [21]). This Maxwell–Wagner effect is essentially a

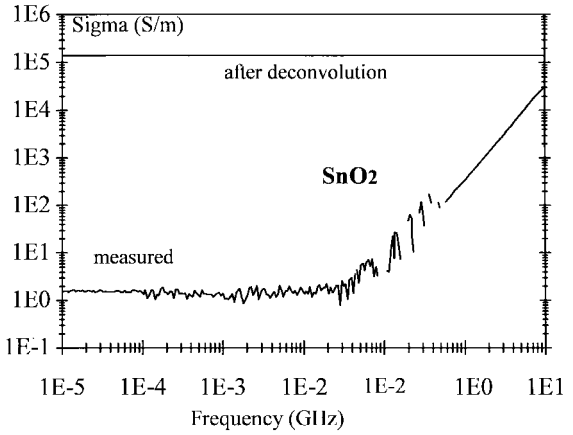

Fig. 11. Conductivity of SnO_2 measured in the bilayered structure formed by the film of SnO_2 ($d_1 = 0.25$ μm) coating an substrate of glass ($d_2 = 1$ mm and $\varepsilon_2 = 7.1 - j0.2$) in APC-7 mm standard.

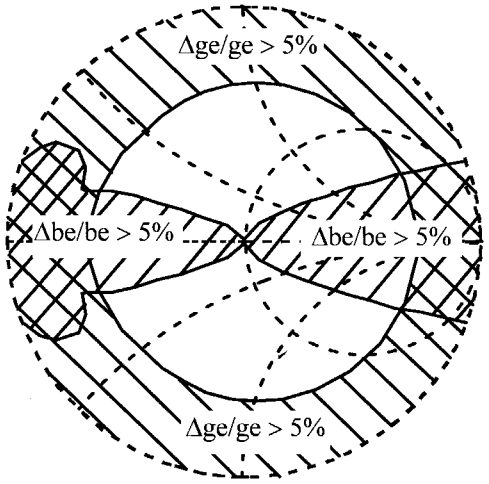

Fig. 12. Example of measurement accuracy at 5%.

combination of resistor–capacitor networks. In this case, the apparent permittivity varies with frequency in a similar way as in the case of Debye dispersion [22] with a relaxation frequency greater than 10 GHz, as shown in Fig. 10 for the higher frequency dispersion. Thus, the observed complex permittivity is a sum of two overlapping dispersions. True electrical parameters of the grain material are then measured only at very high frequencies. The deconvolution of the Cole–Cole diagram as indicated in [14] and [21] gives us the result drawn in Fig. 11, where ac conductivity is constant up to 18 GHz and coincides with the dc measurement, available data [20] and [23].

IV. Discussion and Conclusion

The method accuracy was computed by simulation. The calculator, programmed for HP8510B system instrumentation errors, enables measurement errors $\Delta\varepsilon$ to be determined from measured y_e values. The accuracy of measurements depends on the measured values of y_e. An example of the accuracy provided by the network analyzer is graphed in Fig. 12. Values of b_e or g_e less than 10^{-4} involve errors greater than 100% in the corresponding values of admittance and permittivity.

Hence, the measurement of losses for samples with less than 10^{-2} is difficult with this method. To get reasonable accuracy the loss tangent $\varepsilon''/\varepsilon'$ should be greater than 0.01. In this case, the accuracy for ε' was found to be 3% in the 45 MHz–18 GHz frequency range and ε'' is measured with an accuracy better than 5%. The uncertainty for ε caused by a small error in the sample physical length is practically equal to the percentage of the error. The thin films lengths can be measured by means of interferometric methods.

In this paper, we present a broad-band technique for measuring the complex permittivity for bilayered materials. The method uses an inner-coaxial conductor discontinuity. The electromagnetic analysis is valid irrespective of both bilayered material thickness and working frequency. The capacitive nature of the higher-order modes excited by the discontinuity and their evanescent character allow permittivity measurements for thin films. This system may be employed as a tight cell for dielectric measurements in confined media. Extensive data on different materials have been presented to illustrate the versatility of the present method.

REFERENCES

[1] W. B. Weir, "Automatic measurement of complex dielectric constant and permeability at microwave frequencies," *Proc. IEEE*, vol. 62, pp. 33–36, Jan. 1974.

[2] S. S. Stuchly and M. Matuszewki, "A combined total reflection-transmission method in application to dielectric spectroscopy," *IEEE Trans. Instrum. Meas.*, vol. IM-27, pp. 285–288, Sep. 1978.

[3] J. R. Baker-Jarvis, E. J. Vanzura, and W. A. Kissick, "Improved technique for determining complex permittivity with the transmission/reflection method," *IEEE Trans. Microwave Theory Tech.*, vol. 38, pp. 1096–1103, Aug. 1990.

[4] M. Sucher and J. Fox, *Handbook of Microwave Measurements*, 3rd ed. New York: Wiley, 1963, vol. 2.

[5] E. J. Vanzura, J. R. Baker-Jarvis, J. H. Grosvenor, and M. D. Janezic, "Intercomparison of permittivity measurements using the transmission/reflection method in 7-mm transmission lines," *IEEE Trans. Microwave Theory Tech.*, vol. 42, pp. 2063–2070, Nov. 1994.

[6] C. L. Pournaropulos and D. Misra, "A study on the coaxial aperture electromagnetic sensor and its application in material characterization," *IEEE Trans. Instrum. Meas.*, vol. 43, pp. 111–115, Apr. 1994.

[7] J. Baker-Jarvis, M. D. Janezic, P. D. Domich, and R. G. Geyer, "Analysis of an open-ended coaxial probe with lift-off for nondestructive testing," *IEEE Trans. Instrum. Meas.*, vol. 43, pp. 711–718, Oct. 1994.

[8] N. Belhadj-Tahar and A. Fourrier-Lamer, "Broad-band analysis of coaxial discontinuity used for dielectric measurements," *IEEE Trans. Microwave Theory Tech.*, vol. MTT-34, pp. 346–350, Mar. 1986.

[9] M. Abramowitz and I. A. Stegun, *Handbook of Mathematical Functions*. Washington, DC: Government Printing Office, National Bureau of Standards, Nov. 1970, ch. 9, sec. 4, pp. 369–370.

[10] N. Belhadj-Tahar and A. Fourrier-Lamer, "Utilisation pratique d'une cellule très large bande pour la mesure automatique de la permittivité de divers matériaux," *L'Onde Electrique*, vol. 68, pp. 50–59, Jan. 1988.

[11] P. H. Masterman and P. J. B. Clarricoats, "Computer field-matching solution of waveguide transverse discontinuities," *Proc. Inst. Elect. Eng.*, vol. 118, pp. 51–63, Jan. 1971.

[12] W. J. English, "The circular waveguide step-discontinuity mode transducer," *IEEE Trans. Microwave Theory Tech.*, vol. MTT-21, pp. 633–636, Oct. 1973.

[13] N. Marcuvitz, *Waveguide Handbook*, 1st ed. New York: McGraw-Hill, 1951, sec. 2, pp. 66–80.

[14] F. Buckley and A. A. Maryott, "Tables of Dielectric Dispersion Data for Pure Liquids and Dilute Solutions," Washington, DC: National Bureau of Standard, circular 589, Nov. 1958.

[15] J. H. C. Van Heuven and T. H. A. M. Vlek, "Anisotropy in alumina substrates for microstrip circuits," *IEEE Trans. Microwave Theory Tech.*, vol. MTT-20, pp. 775–777, Nov. 1972.

[16] N. Belhadj-Tahar, A. Fourrier-Lamer, and H. de Chantérac, "Broad-band simultaneous measurement of complex permittivity and permeability using a coaxial discontinuity," *IEEE Trans. Microwave Theory Tech.*, vol. 38, pp. 1–7, Jan. 1990.

[17] S. Jenkins, T. E. Hodgetts, R. N. Clarkes, and A. W. Preece, "Dielectric measurements on reference liquids using automatic network analyzers and calculable geometries," *Meas. Sci. Technol.*, vol. 1, pp. 691–702, Aug. 1990.

[18] A. R. Von Hippel, *Les dielectriques et leurs applications*. Paris, France: Dunod, 1961.

[19] N. Belhadj-Tahar and A. Fourrier-Lamer, "Broad-band simultaneous measurement of complex permittivity and permeability for uniaxial or isotropic materials using a coaxial discontinuity," *J. of Electromagnetic Waves and Applicat.*, vol. 6, pp. 1225–1245, Sept. 1992.

[20] E. E. Kohnke, "Electrical and Optical properties of natural stannic oxide crystals," *J. Phys. Chem. Solids*, vol. 23, pp. 1557–1562, 1962.

[21] A. K. Jonscher, *Dielectric relaxation in solids*. London, UK: Chelsea Dielectrics Press, 1983.

[22] E. Billig and K. W. Plessner, "A note on the dielectric dispersion in polycrystalline materials," *Proc. Phys. Soc.*, vol. 64 B, pp. 361–363, 1951.

[23] K. Ishiguro, T. Sasaki, T. Arai, and I. Imai, "Optical and electrical properties of tin oxide films," *J. Phys. Soc. Japan*, vol. 13, pp. 296–304, Mar. 1958.

Nour-eddine Belhadj-Tahar received the Ph.D. degree (Doctorat de l'Université Pierre et Marie Curie) in electrical engineering from the University Pierre et Marie Curie, PARIS VI, France, in 1986.

From 1980–1982, he was with the Institute of Physics, University of Tlemcen, Algeria, where he held the position of Maître-Assistant. In 1983, he joined the University Pierre et Marie Curie, PARIS VI, France, where he is presently Maître de Conférences. His current research activities include electromagnetic wave propagation in waveguide structures and applications of discontinuities for microwave and millimeter-wave materials characterization.

Olivier Meyer received the Ph.D. degree (Doctorat de l'Université Pierre et Marie Curie) in electrical engineering from the University Pierre et Marie Curie, PARIS VI, France, in 1996.

He is presently an Assistant Professor (Attaché Temporaire d'Enseignement et de Recherche) at the University Pierre et Marie Curie, PARIS VI, France. His research has dealt with microwave dielectric measurement technique and wide-band characterization under microwave heating.

Arlette Fourrier-Lamer received the Ph.D. degree (Doctorat d'Etat ès Sciences Physiques) from the University Pierre et Marie Curie, PARIS IV, France, in 1981.

She is a Professor of Electronic Engineering at the University Pierre et Marie Curie, PARIS VI, France. She was engaged in research on electronic and nuclear double resonance (ENDOR) in paramagnetic liquids until 1981. Since 1982 she has been working on electromagnetic discontinuities and applications to materials characterization (resins, conducting polymers, superconductors, and ferrites). Today, her current areas of interest include nonlinear electromagnetics, wave propagation in chiral media, and microwave processing.

Dr. Fourrier-Lamer is member of the Société Française des Electroniciens et des Radiotechniciens.